Published in final edited form as:
Mol Cell. 2008 October 24; 32(2): 259–275. doi:10.1016/j.molcel.2008.10.002.

Atomic structure of the KEOPS complex: an ancient protein kinase-containing molecular machine

Daniel Y.L. Mao[1,*], **Dante Neculai**[1,*], **Michael Downey**[1,2], **Stephen Orlicky**[1], **Yosr Z. Haffani**[1], **Derek F. Ceccarelli**[1], **Jenny S.L. Ho**[3], **Rachel K. Szilard**[1], **Wei Zhang**[1,2], **Cynthia S. Ho**[1], **Leo Wan**[1], **Christophe Fares**[4], **Sigrun Rumpel**[4], **Igor Kurinov**[5], **Cheryl H. Arrowsmith**[4], **Daniel Durocher**[1,2,§], and **Frank Sicheri**[1,2,§]

[1] Samuel Lunenfeld Research Institute, Mount Sinai Hospital, 600 University Avenue, Toronto, ON, Canada M5G 1X5

[2] Department of Molecular Genetics, University of Toronto, Toronto, Ontario, Canada

[3] Program in Developmental and Stem Cell Biology, The Hospital for Sick Children and University of Toronto, 555 University Avenue, Toronto, ON, Canada, M5G 1X8

[4] Ontario Cancer Institute, Department of Medical Biophysics, University of Toronto, 101 College Street, Toronto, ON, Canada, M5G 1L7

[5] Cornell University, Department of Chemistry and Chemical Biology, NE-CAT, Bldg. 436E, Advanced Photon Source, 9700 S. Cass Ave., Argonne, IL, 60439

SUMMARY

Kae1 is a universally conserved ATPase and part of the essential gene set in bacteria. In archaea and eukaryotes, Kae1 is embedded within the protein kinase-containing KEOPS complex. Mutation of KEOPS subunits in yeast leads to striking telomere and transcription defects but the exact biochemical function of KEOPS is not known. As a first step to elucidating its function, we solved the atomic structure of archaea-derived KEOPS complexes involving Kae1, Bud32, Pcc1 and Cgi121 subunits. Our studies suggest that Kae1 is regulated at two levels by the primordial protein kinase Bud32, which is itself regulated by Cgi121. Moreover, Pcc1 appears to function as a dimerization module, perhaps suggesting that KEOPS may be a processive molecular machine. Lastly, as Bud32 lacks the conventional substrate-recognition infrastructure of eukaryotic protein kinases including an activation segment, Bud32 may provide a glimpse of the evolutionary history of the protein kinase family.

INTRODUCTION

The telomere is a nucleoproteic structure that forms the end of linear chromosomes. In eukaryotes, this structure accomplishes two critical functions. First, telomeres recruit and

[§]Address correspondence to: Frank Sicheri, Ph.D., Centre for Systems Biology, Samuel Lunenfeld Research Institute, Mount Sinai Hospital, Room 1090, 600 University Avenue, Toronto, ON, CANADA M5G 1X5, Tel: 416-586-4800 ext. 8471, Fax: 416-586-8869, sicheri@mshri.on.ca. Daniel Durocher, Ph.D., Centre for Systems Biology, Samuel Lunenfeld Research Institute, Mount Sinai Hospital, Room 1073, 600 University Avenue, Toronto, ON, CANADA M5G 1X5, Tel: 416-586-4800 ext. 2544, Fax: 416-586-8869, durocher@mshri.on.ca.
[*]These authors contributed equally to this work

activate telomerase, a reverse transcriptase that polymerizes short TG-rich repeats on the 3′ end of chromosomes (Gilson and Geli, 2007; Smogorzewska and de Lange, 2004; Verdun and Karlseder, 2007). Second, telomeres protect chromosome ends from nucleolytic degradation, unscheduled DNA repair and activation of the DNA damage checkpoints. This activity, termed telomere capping, is essential for cell viability and genomic integrity (Feldser et al., 2003; Gilson and Geli, 2007; Verdun and Karlseder, 2007).

To identify genes that modulate telomere capping, we screened the viable gene deletion collection of *Saccharomyces cerevisiae* for suppressors of the temperature sensitivity of *cdc13-1* (Downey et al., 2006), an allele of the telomere capping protein Cdc13. This screen identified Cgi121 as a protein that promotes telomere uncapping triggered by *cdc13-1*. Cgi121 is part of a five member complex in yeast termed the KEOPS (or EKC) complex (Downey et al., 2006; Kisseleva-Romanova et al., 2006). In addition to Cgi121, which has no recognizable domains or motifs, the KEOPS complex is composed of a protein kinase, Bud32; a putative ATPase, Kae1 (see below); and two other proteins of small size with no detectable enzymatic function or recognizable domains, Pcc1 and Gon7. The KEOPS complex is conserved in humans, with the exception of Gon7 which could not be detected. Interestingly, human orthologues of Pcc1 have been characterized as cancer antigens, indicating that the upregulation of KEOPS subunits might be associated with cancer.

In addition to promoting telomere uncapping, the KEOPS complex profoundly affects telomere length homeostasis and is required for cell growth in budding yeast. Indeed, deletion of *BUD32* and *GON7* results in dramatic telomere shortening, a drastic reduction in the ability of telomerase to add new telomere sequences to DNA double-strand breaks and severe growth defects. In fact, every component of KEOPS promotes telomere uncapping and elongation (Downey et al., 2006; Gatbonton et al., 2006; Shachar et al., 2008) indicating that the proteins function collectively as a unit.

In parallel, the KEOPS/EKC complex was identified as a novel transcription factor (Kisseleva-Romanova et al., 2006). Components of KEOPS are nuclear proteins that associate with chromatin in vivo and are important for inducible gene transcription (Kisseleva-Romanova et al., 2006). It is not clear how KEOPS promotes transcription but KEOPS mutant yeast strains are defective for the recruitment of coactivators, such as SAGA and Mediator, to target genes. Collectively, these studies indicate that KEOPS promotes the access of nucleases and telomerase to the chromosome end as well as the access of transcriptional complexes to chromatin. A model that explains these seemingly disparate observations is that KEOPS regulates accessibility to chromatin, perhaps by modulating its higher order structure.

Remarkably, the KEOPS component Kae1 is universally conserved in all three domains of life. A Kae1 homolog is present in the smallest bacterial genome, *Mycoplasma genitalium*, in the smallest archaeal genome, *Nanoarchaeum equitans*, and is an essential gene in all bacterial species tested (Arigoni et al., 1998). Kae1 is an ATPase of the ASKHA (acetate & sugar kinase/Hsp70/actin) superfamily. As proteins of this superfamily carry out diverse functions, it is not clear what specific biochemical function Kae1 possesses although *Pasteurella haemolytica* Kae1 can act as an O-sialoglycoprotein protease (Abdullah et al., 1991) and *Pyrococcus abyssi* Kae1 is proposed to be an apurinic (AP) endonuclease (Hecker et al., 2007). Since these two functions are dramatically different, the conserved function of Kae1 remains an open question. No other subunits of KEOPS have been identified in bacteria. However, in archaea, a nearly complete KEOPS complex can be identified (see below). This observation suggests that Kae1-interacting proteins may have evolved to be part of a regulatory infrastructure that modulates the activity of Kae1. Given the importance of KEOPS in telomere biology and gene transcription, and evidence that KEOPS is an

evolutionarily conserved molecular machine, we determined the atomic structure of KEOPS complexes reconstituted from archaeal proteins and probed them for functional significance both in vitro and in vivo. Our findings validate the importance of the KEOPS architecture that we discovered and provide a framework for deciphering the functional relationships between KEOPS subunits.

RESULTS

Architecture of the KEOPS complex

We identified homologs of Pcc1 and Cgi121 in archaea by iterative BLAST searches (Figures S3 & S4). We did not identify a Gon7 homolog in either archaea or the human genome (data not shown). We then determined the underlying architecture of the KEOPS complex using pull down experiments with recombinant forms of archaeal Kae1 (residues 1-328 of *Methanococcus jannaschii* MJ1130); Pcc1 (*Pyrococcus furiosus* PF2011); Cgi121 (*M. jannaschii* MJ0187); or Bud32 (residues 328-535 of MJ1130). Each protein was expressed as a GST fusion in *Escherichia coli* and purified to near homogeneity. The GST tags were used to immobilize proteins on glutathione-Sepharose resin or cleaved with TEV protease, followed by purification, to isolate the untagged protein. GST-Pcc1 immobilized to glutathione resin selectively retained Kae1, but not Bud32 (Figure 1A) or Cgi121 (Figure 1B). In contrast, GST-Cgi121 retained Bud32 but not Kae1 (Figure 1C) while GST-Kae1 retained Bud32 (Figure 1D). Lastly, Bud32 and Cgi121 bound to immobilized GST-Pcc1 only in the presence of Kae1 (Figure 1B) and Kae1 bound to immobilized GST-Cgi121 only in the presence of Bud32 (Figure 1C). These data indicate that KEOPS is organized in a linear fashion where Cgi121 binds to Bud32, which binds to Kae1, which in turn binds to Pcc1. A model depicting the architecture of the KEOPS complex is shown in Figure 1E.

X-ray and NMR structure determination

The linear topology of KEOPS enabled us to crystallize and solve binary and ternary subcomplexes by X-ray crystallography as a means to develop an atomic model of the whole KEOPS complex. We solved a total of six structures using X-ray and NMR methods (see Table 1 & S1 for data collection and refinement statistics). Structure based sequence alignments for Bud32, Kae1, Pcc1, and Cgi121 are shown in Figures S1–5. A composite model for a monomer of the KEOPS complex generated from the subcomplex structures is shown in Figure 1F.

The following sections describe the structure and functional characterizations of the four individual KEOPS subunits followed by characterizations of the three binary interacting pairs of KEOPS subunits. For clarity, the residue numbering corresponds to the *M. jannaschii* proteins (except Pcc1, for which numbers are *P. furiosus*), and, when appropriate, residue numbers corresponding to the *S. cerevisiae* ortholog are shown in parentheses. See Table S3 and Figures S1–5 for residue equivalence.

Individual subunit analyses

i. Bud32 structure and function—The crystal structure of Bud32 reveals a bilobal architecture, characteristic of eukaryotic protein kinases, but with major atypical features (Figure 2A). The N-lobe of canonical protein kinases consists minimally of a five stranded β-sheet and a flanking helix αC. These features are conserved in the primary (Figure S1) and atomic structures of Bud32 (Figure 2A) with the exception of strand β1, which is present but disordered in two different crystal complexes analyzed. The C-lobe of Bud32 is unusually small, consisting of two β-strands (β7 & β8) and five α-helices (αD, αE, αF, αJ & αR) of which only three (αD, αE & αF) have direct equivalents in canonical protein kinase structures (Figure 2A). Strikingly, the C-lobe of Bud32 lacks the infrastructure normally

responsible for phospho-acceptor site recognition, including the activation segment (A-loop), which is substituted by a direct link between strand β8 and helix αF (Figure 2A). Despite its atypical structure, Bud32 retains conserved elements required for ATP binding and catalysis (Figure 2A, Table S2) and indeed can auto-phosphorylate in vitro (Figure 2B) (Facchin et al., 2002) in a manner dependent on the integrity of conserved catalytic elements.

The closest structural homologues of Bud32 are the RIO kinases (Rio1 and Rio2) (Figure 2C, top panel). The Rio kinases also exhibit an abbreviated C-lobe and the absence of an A-loop (for comparison with PKA, which has an A-loop, see Figure 2C, bottom panel). The question of how a protein kinase recognizes and phosphorylates its substrate in the absence of an A-loop remains an open question.

To test the biological importance of unique features identified in archaeal KEOPS structures, we mutated residues in the budding yeast counterpart identified by structure based sequence alignments. These mutants were then introduced into *S. cerevisiae* strains on low copy plasmids in a context where the chromosomal copy of the KEOPS component was deleted. We assessed two biological readouts for KEOPS function: cell growth and telomere length. Consistent with Bud32 being competent for phospho-transfer in vitro, its ATP binding and catalytic residues are required for full biological function in yeast [Figure 2DE, Table S3 & (Downey et al., 2006)]. Indeed, the catalytic cleft mutants K360A (K52A), D467A (D182A), N456A (N166A), D451A (D161A), D451R (D161R), N456A/D467A (N166A/D182) all result in cell growth defects and telomere shortening. The severity of the two phenotypes imparted by the *BUD32* mutations parallel each other, and also parallel the loss of protein kinase activity in vitro caused by the equivalent mutation in archaeal Bud32 (Figure 2B). Interestingly, none of the kinase inactivating mutants displayed phenotypes as strong as *bud32Δ*, indicating that the phosphotransfer activity of Bud32 is not its sole function. Finally, the catalytic cleft mutations tested do not destroy protein structure as each mutant binds archaeal Cgi121 in vitro (Figure S6A) and mutant Bud32 expression levels in yeast are similar to wild type levels (Figure S6B).

ii. Kae1 structure and function—We solved Kae1 structures corresponding to two species (*M. jannaschi*, *T. acidophilum*) in three different protein complexes (Kae1-Bud32, Kae1-Bud32-Cgi121 & Kae1-Pcc1) without nucleotide. The structures of Kae1 are very similar to each other and to the published structure of *P. furiosus* Kae1 (PDB 2IVO, 2IVP and 2IVN) (1.20 Å, 1.17 Å & 1.20 Å C_α rmsd respectively). As the structure of the isolated Kae1 subunit was described previously (Hecker et al., 2007), we only describe features most relevant to this study. Kae1 belongs to the actin-like ATPase domain superfamily of proteins, also known as the ASKHA superfamily. The ASKHA fold serves two broad functions: 1) as conformational hydrolases (e.g. Hsp70, actin) and 2) as metabolite kinases (e.g. glycerol kinase). The ASKHA fold consists of two subdomains (denoted I & II) with highly similar RNase H-like folds (Hurley, 1996). The fold of each subdomain is characterized by a central five strand β-sheet and flanking α-helices. The active site resides in the cleft region between the two subdomains, sandwiched between the two β-sheets. ATP binding is dependent on extensive protein contacts with the adenine ring and sugar. ATPase catalytic function is dependent on bound metal ions. Ribbons and schematic representations in Figures 3AB summarize the conserved nucleotide and metal ion binding infrastructure of Kae1.

The specific function of ASKHA family members is attributable in part to the presence of unique inserts in the core fold (Hurley, 1996). Kae1 possess two unique inserts (denoted specific inserts 1 & 2) that comprise three surface exposed α-helices (α4, α5 & α6) and a long intervening linker between α5 and α6 for the first insert, as well as a C-terminal tail

adopting an extended conformation interspersed by two short 3_{10} helices for the second insert (Figure 3C). The C-terminal tail threads across the catalytic cleft of Kae1. Comparison of Kae1 with other ASKHA family members, with kinase or hydrolase function, did not give insight into its specific function.

To begin our characterization of Kae1, we purified wild type and site-directed mutants of *M. jannaschii* Kae1 and assessed ATP-binding, ATPase activity, DNA binding and AP endonuclease activity. We found that wild type Kae1 binds ATP with a K_d of 27 μM (Table S3), which is well below intracellular ATP levels. We also detected low but reproducible ATPase activity that was not affected by other KEOPS subunits (data not shown) but depended on the presence of metal ion binding residues (Figure S7A). We did not detect apurinic (AP) endonuclease or DNA binding activity (Figure S7B–D). Mutation of residues that coordinate ATP, but not the metal ion, perturbed the ATP-binding function of Kae1 (Table S3). None of the Kae1 mutations destroyed protein fold since all mutant proteins could bind Pcc1 in vitro (Figure S7E). To assess the contribution of ATP- and metal ion-binding to Kae1 biological function, we made *kae1* mutant yeast strains that perturbed one function or the other. *kae1* mutants that perturbed ATP-binding in vitro or that disrupted the putative metal ion binding site, resulted in a phenocopy of the *kae1Δ* mutation in yeast [near absence of cell growth (Figure S7F)] despite wild type protein expression levels (Figure S6C). This effect on yeast growth precluded a full analysis of the telomere length phenotype. However, we were able to culture the ATP-binding mutant (E176R) and, as predicted, this mutant had short telomeres (Figure 3D).

iii. Pcc1 structure and function—The Pcc1 structure was solved alone and in complex with Kae1. The Pcc1 structure consists of a three-stranded anti-parallel β-sheet packed with two α helices on one face, and solvent exposed on the other (Figure 4A top panel). This fold is shared with over 700 functionally diverse proteins (DALI Z score >2.0). A close structural homologue of Pcc1 is the KH domain (Z score=6.7), which functions as a versatile RNA, ssDNA or RNA hairpin binder (Figure S8A). The ability of the KH domain to bind nucleic acids is dependent on a signature motif (GXXG loop), located in a kink in helix α1 (Valverde et al., 2008), which is notably absent in Pcc1 (Figure S8A).

Pcc1 forms a tightly interdigitated dimer with a contact area of 555 $Å^2$ (1110 $Å^2$ buried surface area) (Figure 4AB). Dimerization involves an anti-parallel arrangement of two monomers giving rise to a continuous six-stranded anti-parallel β-sheet packed by four α helices on the same face. Interestingly, this mode of dimerization is widely used by KH domains (Figure S8A). Indeed, Pcc1 dimerizes in solution, under all concentrations tested (Figure S8B). Equilibrium centrifugation analysis of a purified Kae1-Pcc1 complex revealed a 2:2 binding stochiometry (Figure S8C), suggesting that Pcc1 functions as a dimerization module in the presence of other KEOPS subunits. Our attempts to disrupt Pcc1 homo-dimerization by mutation yielded insoluble protein (data not shown), suggesting that Pcc1 is an obligate dimer, a notion supported by the conserved hydrophobic nature of the dimer interface (Figure 4B & S9A).

iv. Cgi121 structure—We solved the structures of human Cgi121 alone as well as archaeal Cgi121 alone and in complex with Bud32 and Kae1 (Figures 4C & 6A). The human and archaeal Cgi121 structures are very similar (2.0Å C_α rmsd), consisting of a central anti-parallel β-sheet abutted by two and five α helices on either face. In surveying the PDB, we identified a close structural ortholog from *P. furiosus* (PDB 1ZD0). Aside from this protein, we did not identify other proteins with a similar fold.

The Kae1-Bud32 interaction

Binding of Bud32 to Kae1 involves a contact surface of 1583 Å^2 (3167 Å^2 buried surface) (Figure 5A) that is highly conserved across Kae1 and Bud32 orthologs (Figure S9BC & S10A). Bud32 engages Kae1 using the forward projecting surfaces of both its N- and C-terminal lobes, which clamps onto subdomain II of Kae1. Overall, the binding mode of Bud32 to Kae1 observed in this study is very similar to the Kae1-Bud32 structure recently reported by Hecker et al. (2008) (PDB 2VWB, 1.75 Å C_α rmsd). Binding to Bud32 does not greatly alter the conformation of Kae1 (1.2 Å C_α rmsd) with the exception of the β3-α1 linker. The reverse cannot be assessed, as we do not have a Bud32 structure in the absence of Kae1.

The N-lobe structural elements of Bud32 involved in Kae1 binding include the C-terminal end of helix αC and its linker to strand β3 (Figure 5B). C-lobe structural elements involved in Kae1 binding include the αE-β7 linker containing the catalytic loop, helix αF, helix αR and the extended C-terminal tail. Kae1 structural elements involved in Bud32 binding include the β3′ strand, the extended linker sequence between helices α5 and α6 (within Kae1-specific insert 1), helix α1′, and helix α2′. The only contacts to subdomain I of Kae1 are mediated by the C-terminal tail of Bud32 which interacts with the C-terminal region of helix α1 and the β4-α2 linker.

The Bud32-Kae1 interface is composed by a mixture of hydrophobic, electrostatic and hydrogen bonding interactions. Interesting interaction clusters include a salt network between Bud32 residues R380 and K365 and Kae1 residues E236 and E233, between Bud32 K489 and Kae1 E148, and between the catalytic base of Bud32, D451, and Kae1 R287. Hydrophobic interactions include a network involving V486 and V482 in Bud32 and L150 and K193 in Kae1 (Figure 5B top panel). Conspicuously, R534 in the C-terminal tail of Bud32 forms a hydrogen bond with N132 in Kae1 immediately adjacent to the metal ion binding site (Figure 5B bottom panel). The R534 interaction correlates with a large displacement of the β3-α1 linker in subdomain I of Kae1, giving rise to a partial opening of the ATP binding cleft and a reduction of inter-subdomain contacts (Figure 5B bottom panel).

To assess the functional significance of the Bud32-Kae1 interaction, we probed the interaction surfaces by site-directed mutagenesis. The K365E, R380E, V486Y, and K489E single site mutations in Bud32 and E233R and E236K single site mutations in Kae1 markedly reduced the Bud32-Kae1 interaction in vitro (Figure 5C) without perturbing binding to Cgi121 and Pcc1 (Figures 5D). In contrast, deletion of the C-terminal tail of Bud32 had no impact on the Bud32-Kae1 interaction (Figure S11A). We then made the equivalent mutations in yeast Kae1 and Bud32 to test for functional relevance in vivo. As shown in Figure S10B and S6C, the Kae1 E233R (E292R) and E236K (E295K) mutations severely impaired growth in budding yeast without adversely affecting protein expression. Similarly, the Bud32 single site mutations K489E (R204E), V486Y (V201Y) and double site mutations K365E/R380E (K57E/R72E) impaired Bud32 function in vivo (Figure S10C) without adversely affecting protein expression (Figure S6B). These results indicate that the binding of Bud32 to Kae1 is critical for KEOPS function, a conclusion also reached by Hecker et al. (2008). As the catalytic base D451 (D161) of Bud32 also lies at the Kae1 contact surface, a perturbation of binding to Kae1 might also explain the more potent in vivo effect caused by the D451R (D161R) mutant relative to other Bud32 active site mutants (Figure 2D). Consistent with this notion, combination mutants targeting both Bud32 catalytic residues and contact residues for Kae1 had more pronounced phenotypic effects approaching the severity of the *BUD32* deletion (Figure S10E, Table S3) without adversely affecting protein expression (Figure S6B). Finally, we tested the importance of the Bud32 C-terminal tail for biological function. Despite the fact that deletion of the tail did not affect

Bud32 binding to Kae1 in vitro, its deletion in yeast Bud32 had a severe growth defect (Figure S6B, Figure S11B). This result suggests a possible role for the Bud32 tail in regulating Kae1 function.

Kae1 may be a substrate of Bud32

Since Kae1 binds close to the catalytic cleft of Bud32, we explored the possibility that Kae1 is a substrate of Bud32. Indeed, Bud32 can phosphorylate Kae1 in vitro (Figure S11C). Secondly, if phosphorylation of Kae1 by Bud32 is functionally relevant, the acceptor sites in Kae1 should be conserved in Kae1 proteins from species containing a Bud32 ortholog. Of 11 conserved S/T residues, T308 and T316 in *M. jannaschii* Kae1 localize to the Kae1-specific insert 2 (Figure S11D). This insert is notable for its meandering path across the catalytic cleft of Kae1 as well as for its conservation across archaeal and eukaryotic Kae1 orthologs but not bacterial counterparts that lack a Bud32 orthologue (Figure S5). The extended and surface exposed nature of the Kae1 insert 2 also leaves it more accessible to the active site of Bud32. In contrast, the remaining 9 conserved S/T sites are deeply buried in the fold of Kae1 or integrated into secondary structure elements.

If Bud32 regulates Kae1 function by phosphorylation of sites within the Kae1-specific insert 2, then deleting the insert might have a pronounced effect in vivo. Supporting this idea, partial (1-372) or full deletion (1-364) of the C-terminal tail of yeast Kae1 caused a severe growth defect (Figure S11E). Moreover, a T308A (T369A) but not T316A (T377A) mutant showed a similar phenotype, without adversely affecting protein expression (Figure S6C). This result is consistent with the notion that T308 (T369) in Kae1 is a Bud32 phospho-regulatory site. Together, these data support the possibility that Kae1 is a biologically relevant substrate of Bud32 and that one phospho-acceptor site lies within the Kae1-specific insert 2. However, deletion of the Kae1-specific insert 2 did not abolish Bud32 phosphorylation of Kae1 in vitro (data not shown), implying that other residues might also be targeted by Bud32 in vitro.

The Bud32-Cgi121 interaction

The binding mode of Cgi121 to Bud32 was revealed in a Bud32-Cgi121-Kae1 ternary structure (Figures 6A & S12A). Cgi121 binds exclusively to the N-lobe of Bud32, to a surface composed by helix αC, the adjacent strand β4 and the β2-β3 linker (Figure 6B). The reciprocal binding surface on Cgi121 is composed by helices α2 and α8. The total contact surface is 700 $Å^2$ (1400 $Å^2$) and relative to the two other inter-subunit contact surfaces of the KEOPS complex, it is the least conserved (Figure S9CD).

The Cgi121-Bud32 interface is composed of a combination of hydrophobic, hydrogen bonding, and electrostatic interactions (Figure 6B). Hydrophobic interactions consist of two clusters. The first is formed by L353 and Y352 at the tip of the Bud32 β2-β3 loop, and L134 in Cgi121 helix α8. The second is formed by A389 and V404 in Bud32 and A138 and L139 in Cgi121. Salt interactions link K392 in Bud32 with D135 in Cgi121, and D403 in Bud32 with K46 in Cgi121. Lastly, Y352 in Bud32 hydrogen bonds with H46 in Cgi121, and K46 in Cgi121 hydrogen bonds with the backbone carbonyl of D403 in Bud32.

Of all inter-subunit contacts characterized, Bud32 displays the largest conformational change upon binding to Cgi121 (1.38 Å C_α rmsd by comparison to 0.9 Å C_α rmsd for Kae1). The most apparent conformational change consists of a 10 Å shift of the β2-β3 loop (Figure S12B). This shift appears stabilized by the involvement of Y352 in Bud32 in both hydrophobic and hydrogen bond interactions with Cgi121. All other N-lobe elements of Bud32 including helix αC and the entire C-lobe appear minimally affected by Cgi121 binding.

Cgi121 stimulates Bud32 activity

We first examined the impact of Cgi121 mutations on the Cgi121-Bud32 interaction. While the L134E, L139R and A138R single site mutations had no effect on Bud32 binding in vitro (Figure 6C) the L134E/A138R double mutation perturbed binding severely. We confirmed by NMR analysis that the overall fold of Cgi121 was not affected by this double mutation (Figure S12C). The dispersed nature of the HSQC spectra produced by the double mutant was consistent with a folded state and the close correspondence of the HSQC spectra produced by wild type and mutant Cgi121 proteins was consistent with the absence of gross structural changes.

The binding of Cgi121 to the Bud32 N-lobe on a site centered on helix αC is reminiscent of the intermolecular mode of Cdk (cyclin-dependent protein kinase) regulation by cyclins (Jeffrey et al., 1995). In the case of Cdks, binding to cyclins reorients helix αC to a productive position that supports catalysis. While the position of αC in Bud32 is not outwardly affected by Cgi121, large conformational changes to the β2-β3 loop are apparent. This led us to test if Cgi121 influences the catalytic activity of Bud32. Cgi121 was a potent activator (>20 fold) of Bud32 auto-phosphorylation in vitro (Figures 2B and 6D). In addition, this activator function was dependent on the ability of Cgi121 to bind Bud32, as the Cgi121 L134E/A138R double mutant did not stimulate Bud32 kinase activity (Figure 6D). To investigate the impact of a loss of binding between Cgi121 and Bud32 in vivo, we made the analogous double mutation (L172E/I176R) in yeast Cgi121. As shown in Figure 6E, the Cgi121 (L172E/I176R) strain displayed a slow growth phenotype in the range of the *cgi121Δ* mutation, strongly suggesting that binding to Bud32 is central to Cgi121's biological function.

A role for Cgi121 in regulating Bud32 protein kinase activity is consistent with the observation that the phenotypes imparted by the *cgi121*Δ mutation are milder than those caused by *bud32Δ* or *kae1Δ* mutations (Downey et al., 2006), and more closely resemble the phenotype of Bud32 catalytic site mutants. Moreover, Cgi121 is expressed at much lower levels than the other members of KEOPS (Ghaemmaghami et al., 2003). This observation is also reminiscent of the cyclin-Cdk paradigm in which the activity of Cdks is regulated by proteosome-mediated destruction of cyclins, while Cdk levels remain fixed. This similarity led us to test if yeast Cgi121 and Bud32 are unstable proteins in *GAL1* promoter shut off experiments. We observed that Cgi121 is highly unstable with a half life of ~30 min whereas Bud32 remained stable during the experiment (Figure 6F). Consistent with the possibility that the binding of Cgi121 to Bud32 enhances its stability in vivo, the expression level of the Cgi121 (L172E/I176R) mutant was unexpectedly low relative to the wild type protein (Figure S6D). Together, these data suggest that Cgi121 may indeed function as a positive regulator of Bud32 function.

The Kae1-Pcc1 interaction

We were unable to crystallize a 2:2 stochiometric complex of Pcc1 with Kae1 but serendipitously crystallized and solved the structure of a 2:1 complex resulting from purification of Kae1 in the presence of an excess of Pcc1 (Figure 7A). Pcc1 and Kae1 do not undergo significant conformational changes in response to complex formation (0.73Å & 1.20Å C_α rmsd, respectively). The Kae1-Pcc1 binding interface is less extensive (contact area: 922 $Å^2$; buried area: 1844 $Å^2$) and less conserved (Figure S9AB) than the Kae1-Bud32 binding interface.

Kae1 binds exclusively to one monomer of the Pcc1 dimer. Kae1 helices α1 and α2 pack against helices α1 and α2 in Pcc1, giving rise to a tightly packed four-helix bundle (Figure S13A). Additional contacts are made between the Kae1 3_{10}-1 helix and the Pcc1 helix α2.

The binding interactions, primarily hydrophobic in nature, are augmented by a small number of salt and hydrogen bonds (Figure S13A). The majority of hydrophobic interactions involve small side chain residues, including T89, A90, T93 on Kae1 and A75, V79, A26 in Pcc1 allowing a close approach of the four participating α helices. Non-hydrophobic contacts include a salt interaction between E30 in Pcc1 and R92 in Kae1.

Consistent with Pcc1 functioning as a dimerization module (Figure S8C), two fully accessible surfaces for Kae1 binding are presented on the Pcc1 dimer structure. Superposition of a second Kae1 molecule onto the free binding surface of Pcc1 revealed contacts involving subdomains II of two juxtaposed Kae1 molecules (Figure S13B). We reason that these contacts would be accommodated by small changes to the inter-subunit closure angle of the Kae1 ASKHA fold to yield the 2:2 stochiometric complex we observed in solution (Figure S8C). Extension of our modeling studies to include Bud32 and Cgi121 in a fully dimeric KEOPS complex revealed no prohibitory contacts involving Cgi121 and Bud32 subunits (Figure S13C).

Functional characterizations of the Kae1-Pcc1 interaction

Introduction of the Kae1 T88R mutation, alone or in combination with T92R or R91E, perturbed binding of Kae1 to Pcc1, but not to Bud32, in vitro (Figures 7B). Mutation of small hydrophobic contact residues in Pcc1 to large polar residues (Pcc1 A75Y and V79R), impaired binding to Kae1, while the double mutant A75Y/V79R had a more pronounced effect (Figure 7C). A charge reversal mutation E30R in Pcc1 also disrupted binding to Kae1. The Pcc1 mutations did not destroy protein fold as each mutant was easily purified (Figure 7D) and eluted as a well behaved dimer during purification (data not shown). Analogous mutations were then made in the yeast *PCC1* and *KAE1* counterparts and introduced into a temperature sensitive *pcc1-4* yeast strain (Kisseleva-Romanova et al., 2006). The Pcc1 V79R (A83R) and A75Y (T79R) mutations that disrupt binding to Kae1 in vitro did not rescue the *pcc1-4* temperature sensitivity phenotype whereas wild type Pcc1 did (Figure 7E, Table S3). Similarly, the T88R (I123R) and R91E (R126A) mutations in Kae1 resulted in severe loss of function in vivo (Figure 7F). Note that the R91E (R126A) Kae1 mutant was expressed well in yeast (Figure S6C). These data indicate that the Pcc1-Kae1 interaction is required for full biological function.

To further test the functional requirement for Pcc1 dimerization in vivo, we made a Pcc1-Pcc1 fusion. The close proximity of the N- and C-termini of adjacent protomers in the Pcc1 homodimer suggested that a Pcc1-Pcc1 fusion would readily form intramolecular dimers. As observed for wild type Pcc1, the Pcc1-Pcc1 wild type fusion rescued the *pcc1-4* temperature sensitive growth phenotype (Figure S13D). Consistent with a need for two functional copies of the Kae1 binding surface on the Pcc1 dimer, disruption of one or both binding sites on the Pcc1-Pcc1 fusion by introduction of A75R (T79R), V79R (A83R) or A75R (T79R)/A75R (T79R) mutations abolished the ability of the Pcc1-Pcc1 fusion to rescue the *pcc1-4* growth defect at the restrictive temperature (Figure S13D). These data are consistent with Pcc1 functioning as a dimer and further suggests that the KEOPS holocomplex acts a dimer *in vivo*. Indeed, the five yeast KEOPS subunits Kae1, Gon7, Pcc1, Cgi121 and Bud32 co-migrate in a complex of apparent MW of ~300,000 Da (Downey et al., 2006); (Downey et al., 2006; Kisseleva-Romanova et al., 2006), which is much larger than a predicted monomer mass of 116,872 Da and more closely matches a predicted dimer mass of 233,744 Da.

DISCUSSION

The KEOPS complex is an ancient, protein kinase-containing molecular machine critical for telomere function and gene transcription in budding yeast. This work provides a framework

for its in-depth functional and biochemical characterization by providing an atomic model of the complex. We also report that the catalytic activity of two KEOPS subunits, Bud32 (protein kinase) and Kae1 (ATPase), along with the four inter-subunit interaction surfaces, are important for the overall function of the KEOPS complex in vivo. A challenge for the future will be to identify the substrate(s) of KEOPS in order to unravel how this molecular machine exerts a profound impact on diverse aspects of cell biology.

Kae1: a universal ASKHA-type ATPase

Kae1 is part of the minimal gene set of all organisms. In eukaryotes, a nuclear encoded Kae1 paralog (Qri7 in *S. cerevisiae*) is localized to mitochondria, itself a bacterial symbiont (Ghaemmaghami et al., 2003; Reinders et al., 2006), underscoring the ancient and critical role that Kae1 must play. ASKHA type ATPases function primarily as either conformational hydrolases or metabolite kinases. Moreover, Kae1 has been proposed to be a glycoprotease and an AP endonuclease, two strikingly different biochemical functions. Our studies with *M. jannaschii* Kae1 revealed ATPase activity but no DNA binding or AP endonuclease activities. Hence, the exact function of Kae1 remains mysterious.

Bud32 as a regulator of Kae1

It is striking that archaeal species produce a single protein encoding both Bud32 and Kae1, indicating an intimate relationship between proteins. Since Kae1 is conserved in all species, it is tempting to speculate that Bud32 (and other members of KEOPS) has evolved to modulate Kae1 function. However, we cannot rule out that Kae1 modulates Bud32 or that Kae1 and Bud32 collaborate to modify other substrates. In fact, Kae1 was recently proposed to be an inhibitor of Bud32 kinase activity (Hecker et al. 2008). Nevertheless, our work suggests two means by which Bud32 may regulate Kae1, first by phosphorylating Kae1, and second by binding Kae1. Dual regulation of Kae1 by Bud32 is experimentally supported by our observation that the *bud32Δ* mutation is phenotypically more severe than disruption of either Bud32 catalytic activity or its binding to Kae1. In fact, a close phenocopy of the *bud32Δ* mutation with *bud32* mutants occurs only when both catalysis and binding to Kae1 are impaired (Figure S10E, Table S3).

ATPases of the ASKHA fold superfamily are often regulated by intermolecular binding partners (Hurley, 1996; Mayer and Bukau, 2005). For example, the low ATPase activity of the *E. coli* chaperone DnaK is enhanced >1000 fold by the binding of peptide substrate and the co-chaperone regulator DnaJ (Liberek et al., 1991). Additionally, the catalytic cycle of DnaK and other ASKHA family ATPases is limited by ADP exchange. This necessitates the action of exchange factors such as GrpE, in the case of DnaK, that opens the nucleotide binding cleft (Harrison et al., 1997).

How does binding of Bud32 influence Kae1 catalytic function? The C-terminal tail of Bud32 binds in the catalytic cleft of Kae1 directly adjacent to the metal ion coordinating center. This leaves the Bud32 tail well placed to influence ATPase activity or binding of a biological substrate. Alternatively the Bud32 induced movement of the β3-α1 linker in Kae1 creates a more open catalytic cleft that might potentiate nucleotide exchange. Investigating these possibilities awaits a better understanding of the biochemical function of Kae1 and the key players in Kae1's catalytic cycle. Indeed, while we detect Kae1 ATPase activity in vitro, the low levels suggest a key factor is missing in our reconstitution assays.

Bud32 and Rio kinase: living protein kinase fossils?

The protein kinase superfamily is a diverse group of enzymes with phospho-transfer activity carried out by an evolutionary conserved bilobal structure. Bud32, along with two Rio paralogs, form the minimal set of protein kinases conserved in all archaeal and eukaryotic

species (Kannan et al., 2007). A general feature of the Rio and Bud32 protein kinases is a minimal C-lobe and absence of an A-loop. The role of the C-lobe and A-loop in substrate recognition raises the question of how Rio and Bud32 kinases recognize their substrates.

We suggest that the higher order binding mode revealed by the Bud32-Kae1 structure may reflect an unconventional kinase substrate targeting mechanism, one involving the recognition of the tertiary fold of the substrate rather than a simple linear peptide motif. This approach to substrate recognition is employed infrequently by canonical eukaryotic protein kinases and has only been visualized at atomic resolution for the eIF2α protein kinase PKR (Dar et al., 2005) and the splicing related kinase SRPK1 (Ngo et al., 2008). The latter kinase-substrate complex is notably similar to the Bud32-Kae1 complex in that the substrate of SRPK1 binds across the front face of the kinase domain in manner that bridges the two kinase lobes.

Our work also identified Cgi121 as a positive regulator of Bud32 kinase activity. This conclusion is based on the stimulatory effect that Cgi121 binding to Bud32 has on Bud32 autocatalytic activity. Moreover, yeast Cgi121 is a substochiometric component of KEOPS and its abundance is regulated by protein degradation. Genetic analysis of *CGI121* in budding yeast is also consistent with it being a positive regulator of KEOPS. We posit that the identification of cellular conditions where Cgi121 is stabilized will provide an important clue as to the core function of the KEOPS complex.

Pcc1: a dimerization subunit

Our study identifies Pcc1 as a dimeric KH domain-like protein. Highlighting the functional importance of Pcc1 in the KEOPS complex, deletion of *PCC1* in yeast results in phenotypes that are as severe as the *BUD32* and *KAE1* deletions (Kisseleva-Romanova et al., 2006). Also, we show that the ability of the Pcc1 dimer to bind two Kae1 molecules is needed for its function in vivo. These data are consistent with our studies that place Pcc1 at the center of a dimeric KEOPS holocomplex. Why KEOPS must function as a dimer remains an open question. One answer to this question might be that KEOPS is a processive molecular machine. Indeed, dimerization and multimerization is a common theme of processive enzymes [e.g. helicases, kinesins, ubiquitin ligases and polymerases (Lohman et al., 1998; Tang et al., 2007)] that perform multiple catalytic cycles on a single substrate. The identification of KEOPS substrate(s) will provide an invaluable tool to decipher the inner workings of this complex, its regulation and its biological function.

EXPERIMENTAL PROCEDURES

Bud32 *in vitro* kinase assays

Bud32 was purified *in vitro* as a hexahistidine tag fusion protein (pProEx-HTa) and concentrated in buffer containing 10 mM HEPES pH 7.5, 300 mM NaCl and 2 mM dithiothreitol (DTT). Kinase assays were performed using [γ-^{32}P]-ATP, 30 μM cold ATP, 20 μM $MnCl_2$ and 0.2–1 μM Bud32 at 60°C. Reactions were resolved by sodium dodecylsulfate polyacrylamide gel electrophoresis (SDS-PAGE) and visualized with a PhosphorImager (Molecular Dynamics).

GST pull down assays

GST-tagged Cgi121, Kae1, or Pcc1 proteins were expressed in *Escherichia coli* BL21 (DE3) Codon Plus cells and lysed in a buffer containing 20 mM HEPES pH 7.5, 300 mM NaCl and 2 mM DTT. Clarified lysate was mixed with glutathione-Sepharose resin at 20°C and allowed to bind for 30 min. 15 μl aliquots of resin bound fusion proteins was incubated with

molar equivalents of purified prey proteins for 30 min, washed 6 times using 100X bed volumes of buffer and resolved by SDS-PAGE.

Plasmids

A description of the plasmids used can be found in the Supplementary Experimental Procedures.

Telomere Length Determination

Telomere length assays were performed as previously described (Downey et al., 2006).

Yeast Strains

See Table S4 for a list of yeast strains. Generation of yeast strains in this study were performed using standard genetic techniques.

Protein Expression, Crystallization and Data Collection

All proteins described in this study were purified using conventional affinity tag purification techniques (either glutathione-Sepharose or nickel chelate chromatography). Affinity were tags removed by TEV protease cleavage where indicated. Seleno-methionine substituted proteins were prepared as described previously (Tang et al., 2007). Heavy atom derivatizations were carried out by soaking crystals in mother liquor solutions containing saturated $[Ta_6Br_{12}]Br_2$. For x-ray diffraction experiments, crystals were flash frozen in mother liquors supplemented with 20–35% (v/v) glycerol. All x-ray data sets were processed using the software XDS (Kabsch, 1993).

Cgi121 isolated structures—The full length *Homo sapiens* and *Methanococcus jannaschii* Cgi121 proteins were expressed in *E. coli* BL21 (DE3) CodonPlus cells as a glutathione S-transferase (GST) fusion protein using a pGEX2T plasmid modified for affinity tag cleavage with the Tobacco Etch Virus (TEV) protease. *H. sapiens* CGi121 crystals of the space group $P6_2$ (a=b=93.56Å, c=87.16Å, α=β=90°, γ=120°) with two molecules in the asymmetric unit were obtained using the hanging drop method by mixing equal volumes of 15 mg/mL protein solution with 20% (w/v) PEG1500, 0.2 M calcium acetate, and 0.1 M imidazole pH 8 at 4°C. A selenium SAD data set was collected at NE-CAT beamline 24-ID-C. NMR analyses on *M. jannaschii* Cgi121 were performed using a Bruker AVANCE 600 or 800 spectrometer at 298K. NMR samples contained 1.6 mM ^{15}N, ^{13}C-labeled *M. jannaschii* CGI121 in 20 mM sodium phosphate pH 6.3 and 100 mM NaCl with 10% D_2O.

Kae1-Bud32 complex—The *Methanococcus jannaschii* protein MJ1130 (Kae1-Bud32 fusion) with an internal deletion of two amino acids (MJ1130 ΔR332-K333) was expressed and purified as an N-terminal GST-fusion protein as per human Cgi121. Crystals of the space group $P4_122$ (a=b=148.73Å, c=136.42Å, α=β=γ=90°) with two molecules in the asymmetric unit were obtained using the hanging drop method by mixing of equal volumes of 6 mg/ml protein solution with 10 mM HEPES pH 7.5, 10% PEG3000 and 11% spermine tetrahydrochloride at 20°C. A tantalum SAD data set was collected at NE-CAT beamline 24-ID-C.

Kae1-Bud32-Cgi121 complex—A 1:1 molar complex of *M. jannaschii* Cgi121 and MJ1130 was obtained by mixing excess molar Cgi121 with MJ1130 followed by size exclusion chromatography to remove excess Cgi121. Crystals of the space group $P2_12_12_1$ (a=76.99Å, b=106.91Å, c=209.99Å, α=β=γ=90°) with two 1:1 complexes of Cgi121 to MJ1130 in the asymmetric unit were obtained using the hanging drop method by mixing

equal volumes of 8 mg/mL of protein complex with 0.1 M MES pH 6.5 and 15% PEG3000. A tantalum SAD data set was collected at NE-CAT beamline 24-ID-C.

Pcc1 structure—Full length *Pyrococcus furiosus* Pcc1 protein (*pfu*Pcc1) was expressed and purified as a N-terminal GST-fusion protein as per human Cgi121. Crystals of the space group $P6_3$ (a=b=78.81Å, c=60.02Å, α=β=90°, γ=120°) with two molecule in the asymmetric unit were obtained using the hanging drop method by mixing of equal volumes of 5 mg/mL protein solution with 45% PEG300, 0.1 M Na/K phosphate pH 6.1 at 20°C. A selenium SAD data set was collected at CHESS East - F2 beamline and processed using the software XDS (Kabsch, 1993).

Kae1-Pcc1 complex—The *Thermoplasma acidophilum* Kae1 protein (*ta*Kae1) was expressed and purified as a N-terminal GST-fusion protein as per human Cgi121. A 2:1 molar complex of *ta*Kae1-*pfu*Pcc1 was obtained by mixing 20 fold molar excess *pfu*Pcc1 with *ta*Kae1 followed by size exclusion chromatography to remove excess Pcc1. Crystals of the space group $P6_5$ (a=b=66.56Å, c=435.56Å, α=β=γ=90°) with two 2:1 complexes of Pcc1:Kae1, respectively, in the asymmetric unit were obtained using the hanging drop method by mixing equal volumes of 5 mg/mL of protein complex with 0.2 M NaCl, 40% PEG300, 0.1 M HEPES pH 7.5 at 20°C. A native data set was collected at NE-CAT beamline 24-ID-E.

X-ray Structure Determinations

For experimental phasing, heavy atoms positions were located using SHELXD (Schneider and Sheldrick, 2002) and refined using SHARP/AUTOSHARP (Vonrhein et al., 2007). RESOLVE (Terwilliger, 2004) was used for density modification and model autobuilding. Coot (Emsley and Cowtan, 2004) was used for all manual building and electron density map inspection. Refinement was carried out using Refmac (Winn et al., 2003) or Phenix (Zwart et al., 2008). The *Hs*Cgi121 and *Pfu*Pcc1 crystal structures were solved by the selenium SAD method. The MJ1130 crystal structure was solved by the tantalum SAD method. The structure of *Mj*Cgi121/MJ1130 complex was solved by a combination of the tantalum SAD method and molecular replacement using Phaser (Storoni et al., 2004). Although the resolution of *Mj*Cgi121/MJ1130 complex analysis was low (3.6 Å) in comparison to the other structure analyses in this study, the high quality of our experimentally phased electron density maps (Figure S6A) in conjunction with our knowledge of the *M. jannaschii* Cgi121 NMR structure allowed us to unambiguously model the position of Cgi121 with respect to Bud32.

The crystal structure of the *Ta*Kae1-*Pfu*Pcc1 complex was solved by molecular replacement using the aforementioned Kae1 and Pcc1 structures as search models in Phaser (Storoni et al., 2004).

*Mj*CGI121 NMR resonance assignment and structure calculation

The 3D spectra were measured with non-uniform sampling (NUS) of the indirect dimensions (down to 30% sampling) and reconstructed using multidimensional decomposition (MDD) using MDDNMR (Jaravine and Orekhov, 2006). All spectra were processed using NMRPipe/NMRDraw (Delaglio et al., 1995) and analyzed using Sparky (Goddard T. D.). Backbone assignments were obtained using standard triple-resonance experiments (Bax and Grzesiek, 1993). Aliphatic side chain assignments were obtained from 3D HCCH-TOCSY and aromatic side chain assignments from 2D (Hβ)Cβ(CγCδ)Hδ and (Hβ)Cβ(CγCδCε)Hε experiments (Yamazaki et al., 1993). Distance restraints, derived from a ^{15}N- and ^{13}C-edited NOESY-HSQC (using cross-relaxation mixing time of 100 ms) and dihedral angle restraints, predicted from chemical shifts with the software TALOS

(Cornilescu et al., 1999; Jaravine and Orekhov, 2006), were used as input for combined automated NOE assignment and structure calculation with the program CYANA (Guntert, 2004). Residual dipolar couplings (RDCs) were gained from the difference between the $^{1}H^{N}$-^{15}N splittings in 2D IPAP-^{1}H-^{15}N HSQC experiments measured under isotropic and anisotropic conditions (Ottiger et al., 1998). Anisotropic media were prepared by addition of filamentous phages to a concentration of 10 mg/mL (Hansen et al., 1998; Zweckstetter and Bax, 2001). The final 20 structures with the lowest target function after the final CYANA cycle were used for further refinement in the presence of 122 HN-RDCs in explicit solvent (Linge et al., 2003). Structure statistics for the 10 lowest energy structures after refinement are shown in Table S1.

Supplementary Material

Refer to Web version on PubMed Central for supplementary material.

Acknowledgments

We thank Steve Bell for help in identifying archaeal KEOPS orthologs and Domenico Libri for strains/plasmids. Research conducted at the NE-CAT beamlines (Advanced Photon Source) was supported by the National Center for Research Resources (NIH, award RR 15301) and the U.S. Department of Energy (Office of Basic Energy Sciences, contract DE-AC02-06CH11357). DD is a Canada Research Chair (Tier II). This work was funded by grants from the CIHR (MOP 79441) to DD and the Canadian Cancer Society to FS (Grant 017220). DYLM and DN were supported by NCIC and CIHR post-doctoral fellowships, respectively. SR was supported by a postdoctoral fellowship of the German Academic Exchange Service (DAAD).

Coordinates have been deposited to the PDB (accession codes 3EN9, 3ENH, 3ENP, 3ENC, 3ENO, 2K8Y).

References

Abdullah KM, Lo RY, Mellors A. Cloning, nucleotide sequence, and expression of the Pasteurella haemolytica A1 glycoprotease gene. J Bacteriol. 1991; 173:5597–5603. [PubMed: 1885539]

Arigoni F, Talabot F, Peitsch M, Edgerton MD, Meldrum E, Allet E, Fish R, Jamotte T, Curchod ML, Loferer H. A genome-based approach for the identification of essential bacterial genes. Nat Biotechnol. 1998; 16:851–856. [PubMed: 9743119]

Bax A, Grzesiek S. Methodological Advances in Protein Nmr. Accounts of Chemical Research. 1993; 26:131–138.

Cornilescu G, Delaglio F, Bax A. Protein backbone angle restraints from searching a database for chemical shift and sequence homology. J Biomol NMR. 1999; 13:289–302. [PubMed: 10212987]

Dar AC, Dever TE, Sicheri F. Higher-order substrate recognition of eIF2alpha by the RNA-dependent protein kinase PKR. Cell. 2005; 122:887–900. [PubMed: 16179258]

Delaglio F, Grzesiek S, Vuister GW, Zhu G, Pfeifer J, Bax A. NMRPipe: a multidimensional spectral processing system based on UNIX pipes. J Biomol NMR. 1995; 6:277–293. [PubMed: 8520220]

Downey M, Houlsworth R, Maringele L, Rollie A, Brehme M, Galicia S, Guillard S, Partington M, Zubko MK, Krogan NJ, et al. A genome-wide screen identifies the evolutionarily conserved KEOPS complex as a telomere regulator. Cell. 2006; 124:1155–1168. [PubMed: 16564010]

Emsley P, Cowtan K. Coot: model-building tools for molecular graphics. Acta crystallographica. 2004; 60:2126–2132.

Facchin S, Lopreiato R, Stocchetto S, Arrigoni G, Cesaro L, Marin O, Carignani G, Pinna LA. Structure-function analysis of yeast piD261/Bud32, an atypical protein kinase essential for normal cell life. Biochem J. 2002; 364:457–463. [PubMed: 12023889]

Feldser DM, Hackett JA, Greider CW. Telomere dysfunction and the initiation of genome instability. Nat Rev Cancer. 2003; 3:623–627. [PubMed: 12894250]

Gatbonton T, Imbesi M, Nelson M, Akey JM, Ruderfer DM, Kruglyak L, Simon JA, Bedalov A. Telomere length as a quantitative trait: genome-wide survey and genetic mapping of telomere length-control genes in yeast. PLoS Genet. 2006; 2:e35. [PubMed: 16552446]

Ghaemmaghami S, Huh WK, Bower K, Howson RW, Belle A, Dephoure N, O'Shea EK, Weissman JS. Global analysis of protein expression in yeast. Nature. 2003; 425:737–741. [PubMed: 14562106]

Gilson E, Geli V. How telomeres are replicated. Nat Rev Mol Cell Biol. 2007; 8:825–838. [PubMed: 17885666]

Goddard, TD.; KDG. SPARKY. Vol. 3. University Of California; San Francisco:

Guntert P. Automated NMR structure calculation with CYANA. Methods Mol Biol. 2004; 278:353–378. [PubMed: 15318003]

Hansen MR, Mueller L, Pardi A. Tunable alignment of macromolecules by filamentous phage yields dipolar coupling interactions. Nature Structural Biology. 1998; 5:1065–1074.

Harrison CJ, Hayer-Hartl M, Di Liberto M, Hartl F, Kuriyan J. Crystal structure of the nucleotide exchange factor GrpE bound to the ATPase domain of the molecular chaperone DnaK. Science. 1997; 276:431–435. [PubMed: 9103205]

Hecker A, Leulliot N, Gadelle D, Graille M, Justome A, Dorlet P, Brochier C, Quevillon-Cheruel S, Le Cam E, van Tilbeurgh H, et al. An archaeal orthologue of the universal protein Kae1 is an iron metalloprotein which exhibits atypical DNA-binding properties and apurinic-endonuclease activity in vitro. Nucleic Acids Res. 2007; 35:6042–6051. [PubMed: 17766251]

Hurley JH. The sugar kinase/heat shock protein 70/actin superfamily: implications of conserved structure for mechanism. Annu Rev Biophys Biomol Struct. 1996; 25:137–162. [PubMed: 8800467]

Jaravine VA, Orekhov VY. Targeted acquisition for real-time NMR spectroscopy. Journal of the American Chemical Society. 2006; 128:13421–13426. [PubMed: 17031954]

Jeffrey PD, Russo AA, Polyak K, Gibbs E, Hurwitz J, Massague J, Pavletich NP. Mechanism of CDK activation revealed by the structure of a cyclinA-CDK2 complex. Nature. 1995; 376:313–320. [PubMed: 7630397]

Kabsch W. Automatic processing of rotation diffraction data from crystals of initially unknown symmetry and cell constants. Journal of Applied Crystallography. 1993; 26:795–800.

Kannan N, Taylor SS, Zhai Y, Venter JC, Manning G. Structural and functional diversity of the microbial kinome. PLoS Biol. 2007; 5:e17. [PubMed: 17355172]

Kisseleva-Romanova E, Lopreiato R, Baudin-Baillieu A, Rousselle JC, Ilan L, Hofmann K, Namane A, Mann C, Libri D. Yeast homolog of a cancer-testis antigen defines a new transcription complex. Embo J. 2006; 25:3576–3585. [PubMed: 16874308]

Liberek K, Marszalek J, Ang D, Georgopoulos C, Zylicz M. Escherichia coli DnaJ and GrpE heat shock proteins jointly stimulate ATPase activity of DnaK. Proc Natl Acad Sci U S A. 1991; 88:2874–2878. [PubMed: 1826368]

Linge JP, Williams MA, Spronk CA, Bonvin AM, Nilges M. Refinement of protein structures in explicit solvent. Proteins. 2003; 50:496–506. [PubMed: 12557191]

Lohman TM, Thorn K, Vale RD. Staying on track: common features of DNA helicases and microtubule motors. Cell. 1998; 93:9–12. [PubMed: 9546385]

Mayer MP, Bukau B. Hsp70 chaperones: cellular functions and molecular mechanism. Cell Mol Life Sci. 2005; 62:670–684. [PubMed: 15770419]

Ngo JC, Giang K, Chakrabarti S, Ma CT, Huynh N, Hagopian JC, Dorrestein PC, Fu XD, Adams JA, Ghosh G. A sliding docking interaction is essential for sequential and processive phosphorylation of an SR protein by SRPK1. Mol Cell. 2008; 29:563–576. [PubMed: 18342604]

Ottiger M, Delaglio F, Bax A. Measurement of J and dipolar couplings from simplified two-dimensional NMR spectra. Journal of Magnetic Resonance. 1998; 131:373–378. [PubMed: 9571116]

Reinders J, Zahedi RP, Pfanner N, Meisinger C, Sickmann A. Toward the complete yeast mitochondrial proteome: multidimensional separation techniques for mitochondrial proteomics. J Proteome Res. 2006; 5:1543–1554. [PubMed: 16823961]

Schneider TR, Sheldrick GM. Substructure solution with SHELXD. Acta crystallographica. 2002; 58:1772–1779.

Shachar R, Ungar L, Kupiec M, Ruppin E, Sharan R. A systems-level approach to mapping the telomere length maintenance gene circuitry. Mol Syst Biol. 2008; 4:172. [PubMed: 18319724]

Smogorzewska A, de Lange T. Regulation of telomerase by telomeric proteins. Annu Rev Biochem. 2004; 73:177–208. [PubMed: 15189140]

Storoni LC, McCoy AJ, Read RJ. Likelihood-enhanced fast rotation functions. Acta crystallographica. 2004; 60:432–438.

Tang X, Orlicky S, Lin Z, Willems A, Neculai D, Ceccarelli D, Mercurio F, Shilton BH, Sicheri F, Tyers M. Suprafacial orientation of the SCFCdc4 dimer accommodates multiple geometries for substrate ubiquitination. Cell. 2007; 129:1165–1176. [PubMed: 17574027]

Terwilliger T. SOLVE and RESOLVE: automated structure solution, density modification and model building. Journal of synchrotron radiation. 2004; 11:49–52. [PubMed: 14646132]

Valverde R, Edwards L, Regan L. Structure and function of KH domains. Febs J. 2008; 275:2712–2726. [PubMed: 18422648]

Verdun RE, Karlseder J. Replication and protection of telomeres. Nature. 2007; 447:924–931. [PubMed: 17581575]

Vonrhein C, Blanc E, Roversi P, Bricogne G. Automated structure solution with autoSHARP. Methods in molecular biology (Clifton, NJ). 2007; 364:215–230.

Winn MD, Murshudov GN, Papiz MZ. Macromolecular TLS refinement in REFMAC at moderate resolutions. Methods in enzymology. 2003; 374:300–321. [PubMed: 14696379]

Yamazaki T, Forman-Kay JD, Kay LE. Two-dimensional NMR experiments for correlating 13C-beta and 1H-delta/epsilon chemical shifts of aromatic residues in 13C-labeled proteins via scalar couplings. J Am Chem Soc. 1993; 115:11054–11055.

Zwart PH, Afonine PV, Grosse-Kunstleve RW, Hung LW, Ioerger TR, McCoy AJ, McKee E, Moriarty NW, Read RJ, Sacchettini JC, et al. Automated structure solution with the PHENIX suite. Methods in molecular biology (Clifton, NJ). 2008; 426:419–435.

Zweckstetter M, Bax A. Characterization of molecular alignment in aqueous suspensions of Pf1 bacteriophage. Journal of Biomolecular Nmr. 2001; 20:365–377. [PubMed: 11563559]

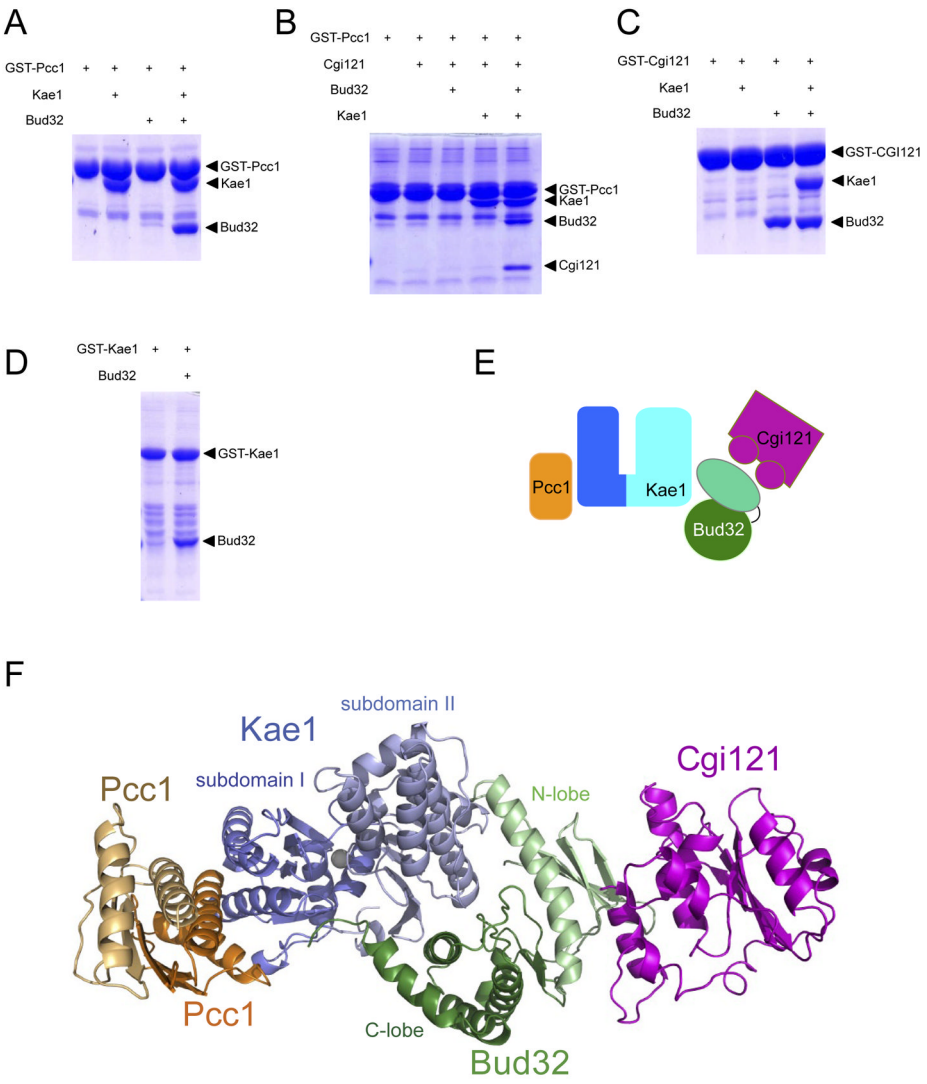

Figure 1. Architecture of the KEOPS complex

(A–D) GST pull down experiments with purified KEOPS subunits. Proteins were separated by SDS-PAGE and visualized by Coomassie blue staining.

(E) Architectural model of the KEOPS complex derived from (A–D).

(F) Composite model of the KEOPS complex based on the X-ray crystal structures of single subunits, binary complexes and a ternary complex summarized in Table 1.

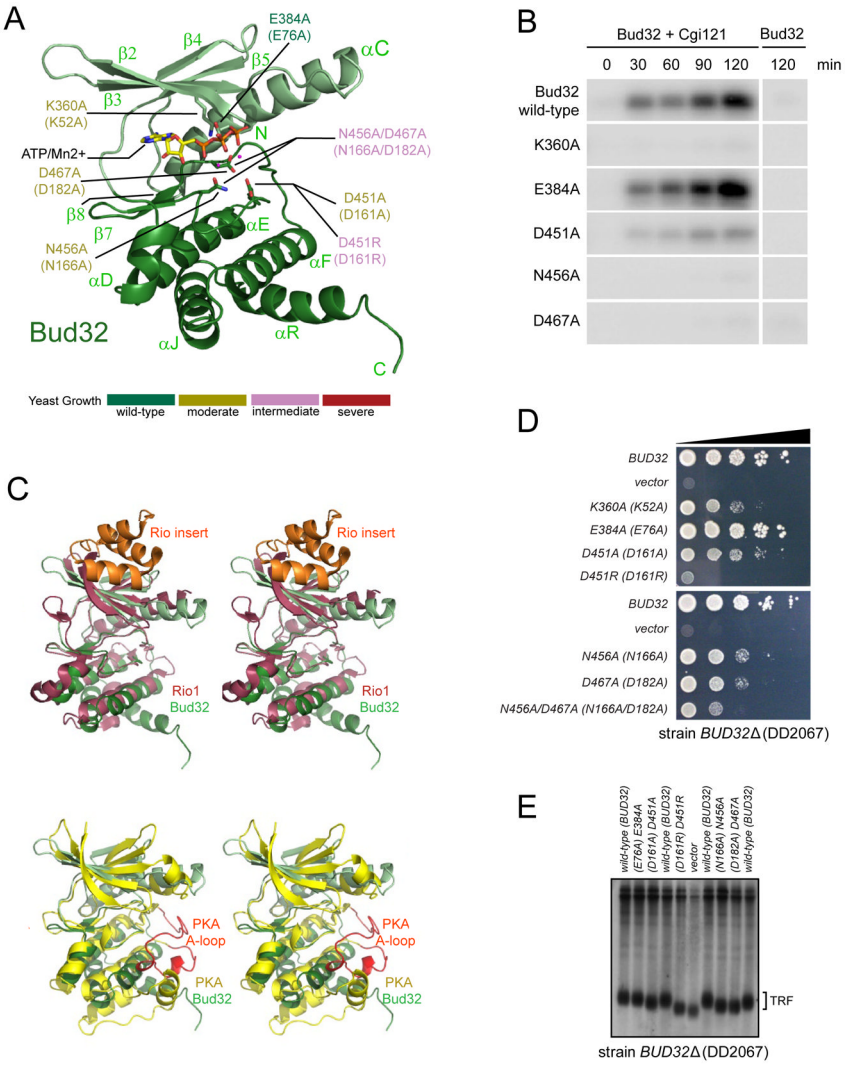

Figure 2. Structure and catalytic function of Bud32

(A) Ribbons representation of Bud32 showing important catalytic residues. For all figures and tables, residues of the archaeal ortholog are listed first and when appropriate, that of the *S. cerevisiae* ortholog are bracketed. Residue labels are colored according to the effect of the indicated mutations on growth in yeast (see color legend). The N-lobe of Bud32 is colored light green and the C-lobe is colored dark green. A metal ion and ATP were modeled into the catalytic cleft based on the structure of RIO1 (PDB 1ZP9).

(B) Autophosphorylation analysis of Bud32 wild type or mutant proteins in the presence or absence of Cgi121. Assays were carried out with [γ-^{32}P]-ATP at 60°C and stopped at the indicated time points. Products of the reactions were separated by SDS-PAGE and ^{32}P incorporation was detected by autoradiography.

(C) Ribbons comparison of Bud32 with Rio1 (PDB 1ZP9; top panel) and PKA (PDB 2CPK; bottom panel). Bud32 is colored as in (A) and Rio kinase is shown in red with its unique N-terminal lobe insertion (labeled as 'Rio insert') in orange. PKA is colored yellow with its A-loop shown in red.

(D) Effect of Bud32 catalytic cleft mutations on the growth of yeast. A *bud32Δ* yeast strain was transformed with a centromeric low copy vector expressing wild type *BUD32*, the indicated Bud32 mutant or the empty vector as control. Liquid cultures of each strain were

spotted on minimal medium in a series of 10 fold dilutions. Growth of yeast at 30°C was monitored over a 6 day period. Representative data is shown. A summary of doubling times in liquid culture for a selection of mutants is provided in Table S3.
(E) Bud32 catalytic mutants have short telomeres. Terminal restriction fragment (TRF) analysis of the yeast strains described in (D).

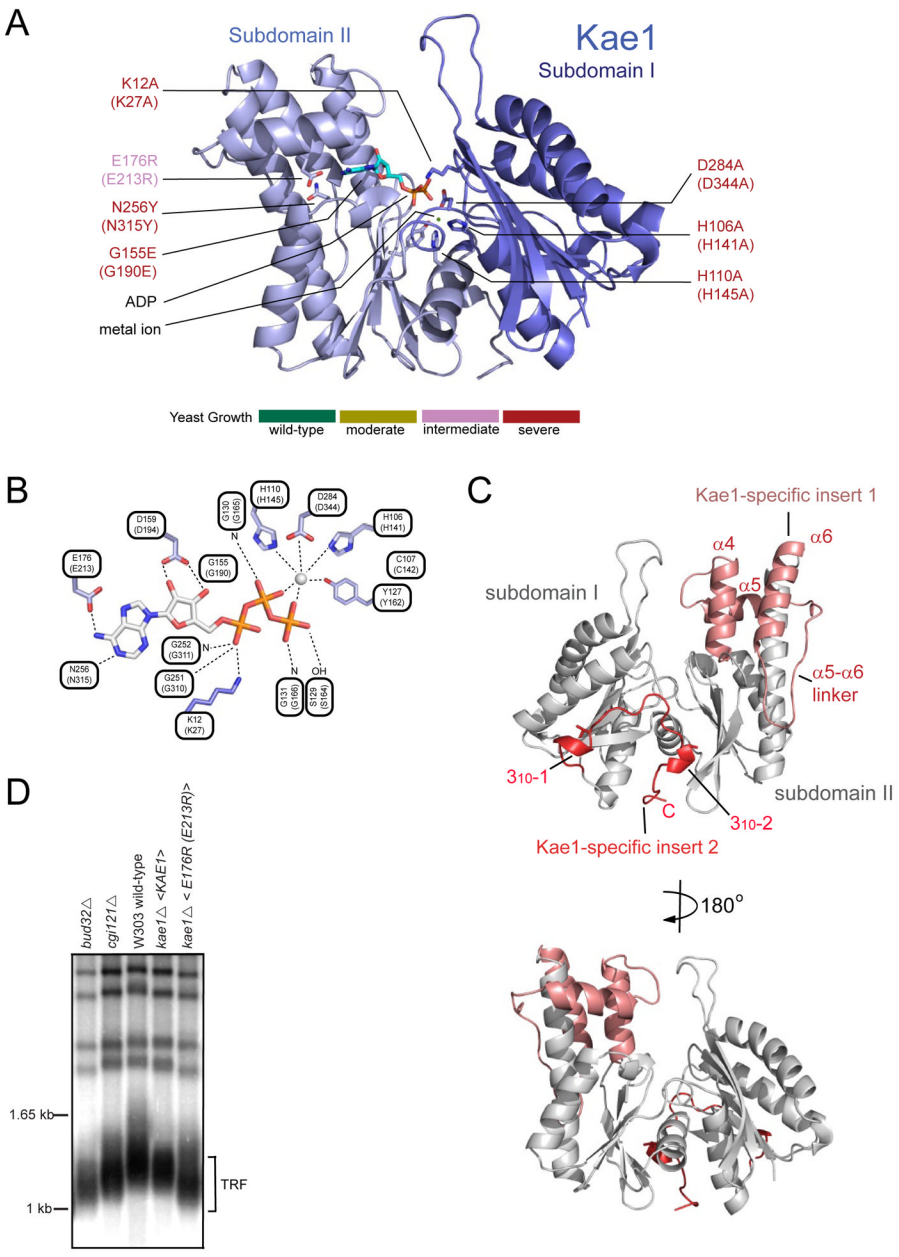

Figure 3. Structure and catalytic function of Kae1

(A) Ribbons representation of Kae1 highlighting catalytic cleft residues. Subdomains I and II are colored dark and light blue respectively. The metal ion and ADP were modeled into the cleft based on the structure of *P. abyssi* Kae1 (PDB 2IVP).

(B) Schematic of catalytic cleft residues of Kae1 that coordinate ATP and metal ion (based on PDB 2IVP).

(C) Kae1 has two characteristic inserts (colored pink and red) that distinguish it from other ASKHA fold proteins. Secondary structure elements within the unique inserts are labeled.

(D) The *kae1-E176R (E213R)* mutant has short telomeres. TRF analysis was performed on the *kae1Δ* strain transformed with a low copy vector encoding wild type Kae1 or the E176 (E213R) mutant. Telomeres from wild type, *bud32Δ* and *cgi121Δ* strains were used as reference.

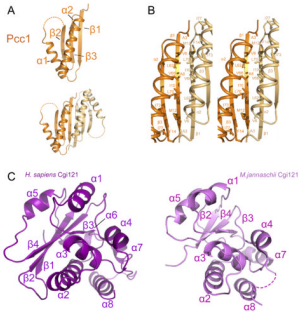

Figure 4. Structures of Pcc1 and Cgi121

(A) Ribbons representation of the Pcc1 monomer (top) and dimer (bottom). Pcc1 protomers 1 and 2 are colored light and dark orange respectively.

(B) Stereo view of conserved hydrophobic contacts within the Pcc1 dimer interface.

(C) Ribbons representation of human Cgi121 (left) and *M.jannaschii* Cgi121 (right) (rmsd=1.92 Å).

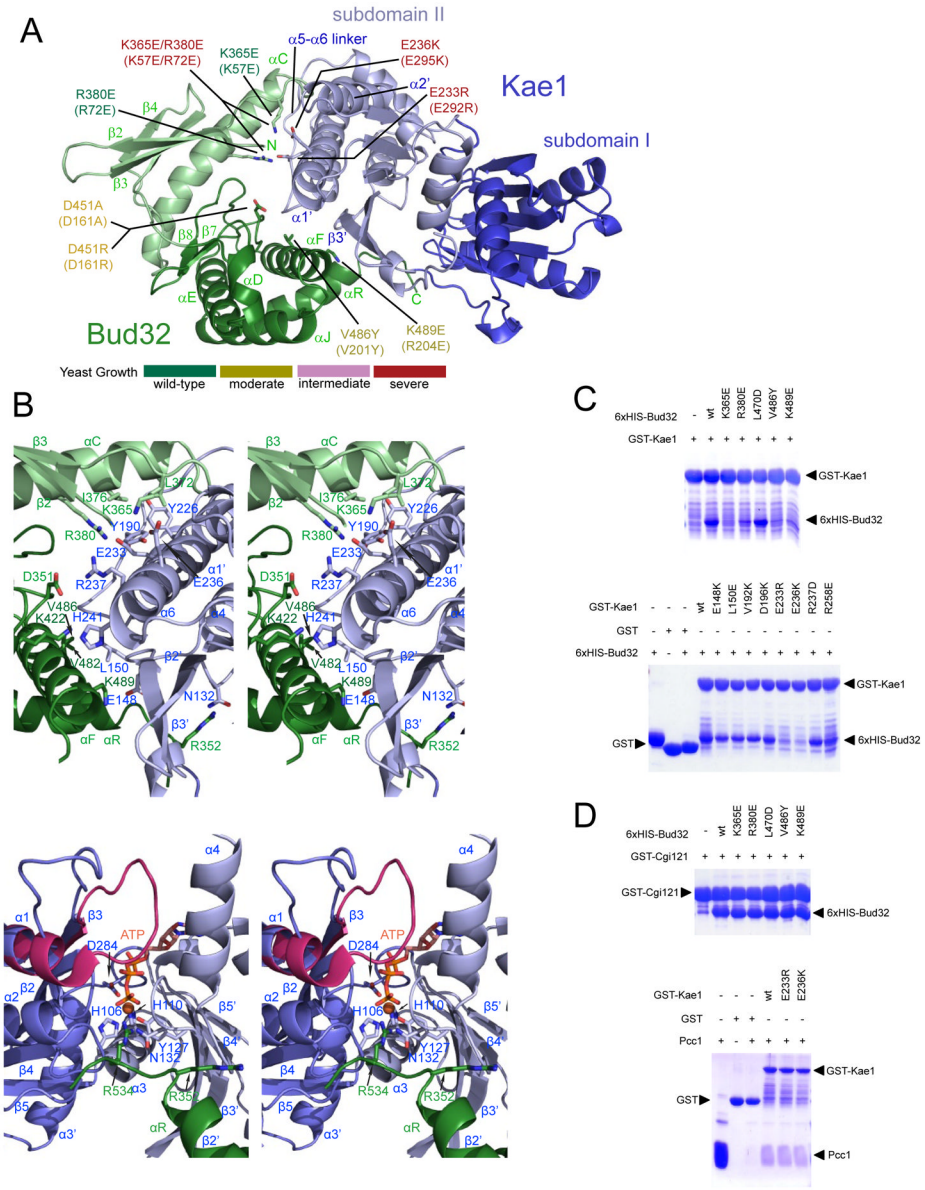

Figure 5. Binding mode of Bud32 to Kae1

(A) Ribbons representation of the Bud32-Kae1 complex. Kae1 and Bud32 are colored as in Figures 2A and 3A. Interface residues whose mutation gives rise to growth phenotypes in yeast are shown in stick representation.

(B) Stereo zoom-in view of the Kae1-Bud32 binding interface centered on (top) Kae1-specific insert 1 and (bottom) C-terminal tail region of Bud32. Figures are colored as in (A).

(C,D) Mutation of the Kae1-Bud32 binding interface. Binding experiments with the indicated GST fusion baits and prey proteins were performed as in Figure 1. (C) Examination of the Bud32-Kae1 interaction. Lane 1 (lower panel) is a loading control for Bud32. (D) Examination of the Cgi121-Bud32 interaction using Bud32 mutants (top) and the Pcc1-Kae1 interaction using Kae1 mutants (bottom).

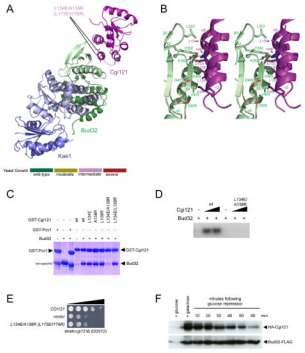

Figure 6. Binding mode of Cgi121 to Bud32

(A) Ribbons representation of the Cgi121-Bud32-Kae1 complex. Bud32, Kae1 and Cgi121 are colored as in Figures 2A, 3A and 4B, respectively. Residues whose mutation gives rise to strong phenotypes in yeast are highlighted.

(B) Stereo zoom-in view of the Bud32-Cgi121 binding interface showing side chains that participate in the interaction.

(C) In vitro binding experiments with the indicated GST fusion baits and purified prey proteins.

(D) Disruption of Cgi121 binding to Bud32 impairs the ability of Cgi121 to potentiate Bud32 autophosphorylation activity in vitro. Bud32 kinase reactions were performed as in Figure 2B.

(E) Functional analysis in yeast of Bud32-Cgi121 binding interface mutations on cell growth. *cgi121Δ* yeast was transformed with empty vector, a vector encoding wild type Cgi121 or the L134E/A138R (L172E/I176R) double mutant. All strains were plated by serial dilution on minimal medium as described in Figure 2D.

(F) Analysis of Cgi121 and Bud32 stability in vivo. Yeast encoding galactose-inducible 3xHA-Cgi121 and Bud32-FLAG proteins were grown for 4 hrs in media containing 2% glucose or 2% galactose. Cells grown in galactose were washed and resuspended in 2% glucose-containing media to repress the *GAL1* promoter. Cells were harvested at times following glucose addition. α-HA and α-FLAG immunoblots are shown.

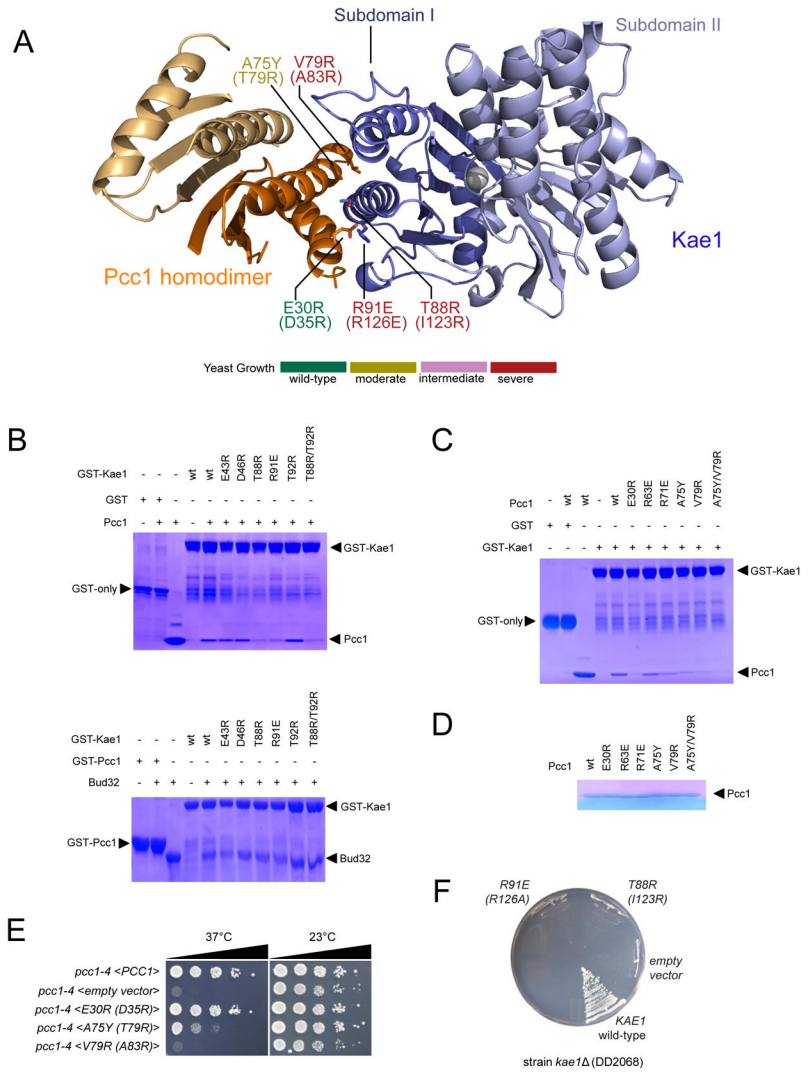

Figure 7. Binding mode of Pcc1 to Kae1

(A) Ribbons representation of the binding interface between Pcc1 and Kae1. Pcc1 and Kae1 are colored as in Figures 3 and 4, respectively. Residues whose mutation gives rise to a phenotype in yeast are highlighted. See Figure S13A for a zoom-in view of the Pcc1-Kae1 binding interface with participating side chains.

(B–D) Mutational analysis of the Pcc1-Kae1 binding interface. Binding experiments with the indicated GST fusion baits and prey proteins were performed as in Figure 1. (B) Examination of various Kae1 proteins binding to Pcc1 (upper panel) or Bud32 (lower panel). (C) Examination of various Pcc1 proteins binding to Kae1. (D) Input gel shows equivalent quantities of soluble wild type and mutant Pcc1 proteins used in the binding reactions in (C).

(E) Analysis of Kae1-Pcc1 interface mutations on yeast growth. Left panel: Serial dilutions of thermosensitive *pcc1-4* strains harboring plasmid encoding wild type Pcc1, pcc1 mutants or empty vector were grown at 37°C (non-permissive) or 23°C (permissive) for 3–5 days. Right panel: *kae1Δ* yeast harboring plasmid encoding wild type Kae1, Kae1 mutants or empty vector were grown for 3–6 days.

Table 1

Data collection and refinement statistics.

	***mj*Bud32/Kae1**	***mj*Bud32/Kae1/*mj*Cgi121**	***hs*Cgi121**	***pfu*Pcc1**	***ta*Kae1/*pfu*Pcc1**
Wavelength (Å)	0.97888	0.97888	0.9793	0.979	0.97935
Resolution (Å)	2.67	3.6	2.48	2.63	3.02
Rsym (%)	5.78 (22.86)	7.59(18.38)	5.6(31.17)	3.31(26.77)	9.50 (44.59)
Total Reflections	82971	20745	29584	12370	76617
Unique Reflections	43971	20745	15455	6413	21362
Completeness (%)	99.8 (100)	99.7(99.8)	99.8(99.1)	97.3(66.1)	99.9(99.7)
I/σ	20.06 (3.4)	14.21(3.67)	14.84(2.24)	24.16(2.86)	16.43(2.43)
Twin Law, Twin fraction				h,-h-k,-l, 0.49	h,-h-k,-l 0.489
Refinement					
Resolution range (Å)	150–2.9	95–3.6	31.8–2.48	68.25–2.63	39.6–3.02
Reflections	43966	19689	15398	6390	21252
Rfactor/Rfree (%)	20.96/26.79	27.64(32.55)	22.40(28.78)	19.2(22.2)	20.14(24.71)
Rms deviations					
Bonds (Å)	0.026	0.047	0.003	0.082	0.003
Angles (°)	0.825	1.375	0.644	1.232	0.706
Space group	$P4_122$ a=b=148.73Å, c=136.42 Å	$P2_12_12_1$ a=76.99Å b=106.91Å, c=209.99Å	$P6_2$ a=b=93.521Å, c=87.155Å	$P6_3$ a=b=78.81Å, c=60.02 Å	$P6_5$ a=b=66.56Å, c=435.56 Å
Molelcules *per* a.u.(rmsd)	2 (1.20 Å)	2 (0.50 Å)	2(0.04 Å)	2(0.78 Å)	2 (0.02 Å)
Ramachandran Data					
Most favored	89.8%	82.6%	92.0%	84.9%	84.6%
Additionally allowed	9.6%	17.2%	8.0%	14.4%	14.8%
Generously allowed	0.5 %	0.2%	0%	0.7%	0.6%
Disallowed	0%	0%	0%	0%	0%

$R_{sym} = \Sigma_h \Sigma_i | I_{h,i} - I_h | / \Sigma_h \Sigma_i I_{h,i}$, where I_h is the mean intensity of the i observations of symmetry related reflections of h. $R = \Sigma | F_{obs} - F_{calc} | / \Sigma F_{obs}$, where $F_{obs} = F_P$ and F_{calc} is the calculated protein structure factor from the atomic model.